The no-spin zone: rotation vs dispersion support in observed and simulated dwarf galaxies

Coral Wheeler[1]*, Andrew B. Pace[1], James S. Bullock[1], Michael Boylan-Kolchin[2]
Jose Oñorbe[3], Alex Fitts[2], Philip F. Hopkins[4], Dušan Kereš[5]

[1]*Center for Cosmology, Department of Physics and Astronomy, University of California, Irvine, CA 92697, USA*
[2]*Department of Astronomy, The University of Texas at Austin, 2515 Speedway, Stop C1400, Austin, TX 78712*
[3]*Max-Planck-Institut fuer Astronomie, Koenigstuhl 17, 69117 Heidelberg, Germany*
[4]*TAPIR, Mailcode 350-17, California Institute of Technology, Pasadena, CA 91125, USA*
[5]*Department of Physics, Center for Astrophysics and Space Sciences, University of California at San Diego, 9500 Gilman Drive, La Jolla, CA 92093*

5 November 2015

ABSTRACT

We perform a systematic Bayesian analysis of rotation vs. dispersion support ($v_{\rm rot}/\sigma$) in 40 dwarf galaxies throughout the Local Volume (LV) over a stellar mass range $10^{3.5}\,{\rm M_\odot} < {\rm M_\star} < 10^8\,{\rm M_\odot}$. We find that the stars in ∼ 90% of the LV dwarf galaxies studied – both satellites and isolated systems – are dispersion-supported. In particular, we show that 7/10 *isolated* dwarfs in our sample have stellar populations with $v_{\rm rot}/\sigma < 0.6$. All have $v_{\rm rot}/\sigma \lesssim 2$. These results challenge the traditional view that the stars in gas-rich dwarf irregulars (dIrrs) are distributed in cold, rotationally-supported stellar disks, while gas-poor dwarf spheroidals (dSphs) are kinematically distinct in having dispersion-supported stars. We see no clear trend between $v_{\rm rot}/\sigma$ and distance to the closest L$_\star$ galaxy, nor between $v_{\rm rot}/\sigma$ and $M_\star$ within our mass range. We apply the same Bayesian analysis to four FIRE hydrodynamic zoom-in simulations of isolated dwarf galaxies ($10^9\,{\rm M_\odot} < {\rm M_{vir}} < 10^{10}\,{\rm M_\odot}$) and show that the simulated *isolated* dIrr galaxies have stellar ellipticities and stellar $v_{\rm rot}/\sigma$ ratios that are consistent with the observed population of dIrrs *and* dSphs without the need to subject these dwarfs to any external perturbations or tidal forces. We posit that most dwarf galaxies form as puffy, dispersion-supported systems, rather than cold, angular momentum-supported disks. If this is the case, then transforming a dIrr into a dSph may require little more than removing its gas.

Key words: galaxies: dwarf – galaxies: formation – galaxies: star formation – galaxies: kinematics and dynamics – Local Group

1 INTRODUCTION

Dwarf spheroidal (dSph) galaxies comprise the largest population of galaxies in the Local Group, consisting of nearly 60 confirmed members (Kleyna et al. 2005; Muñoz et al. 2006a; Martin et al. 2007; Simon & Geha 2007; Simon et al. 2011, 2015; Adén et al. 2009; Belokurov et al. 2009; Carlin et al. 2009; Geha et al. 2009; Koch et al. 2009; Walker et al. 2009, 2015; Kalirai et al. 2010; Collins et al. 2010, 2011; Koposov et al. 2011, 2015a,b; Willman et al. 2011; Tollerud et al. 2012; Collins et al. 2013; Kirby et al. 2013; Kirby, Simon & Cohen 2015; Kirby et al. 2015; Tollerud et al. 2013; Laevens et al. 2015a,b; Kim et al. 2015; Kim & Jerjen 2015; Martin et al. 2015a,b). These objects are characterized by their low luminosities, spheroidal shapes, high mass-to-light ratios, and by the absence of appreciable gas or recent star formation (Ferguson & Binggeli 1994; van den Bergh 1999; Mateo 1998; Dal-

canton, Yoachim & Bernstein 2004; Yoachim & Dalcanton 2006; McConnachie 2012). Line of sight velocity measurements suggest that dSphs have little to no rotation in their stellar populations and velocity dispersion profiles that are nearly flat with radius (Wilkinson et al. 2004; Muñoz et al. 2005, 2006b; Walker et al. 2006, 2007; Koch et al. 2007b,a; Mateo, Olszewski & Walker 2008).

In the Local Group, dSphs tend to occupy regions close to either the Milky Way or M31 (Mateo 1998; Grebel 1999). At greater distances from the two massive galaxies, the population of dSphs dwindles and gives way to a different class of low-mass galaxies called dwarf irregulars (dIrrs). These galaxies have similar luminosities to dSphs, but are distinct most notably in that they have retained some of their gas. Many dIrrs also demonstrate disky features and rotation in their HI content (Mateo 1998; McConnachie 2012). This "Local Group morphology-density relation," with dSphs found close and dIrrs found far from MW and M31, mimics similar relationships between galaxy shape and distance from the local barycenter found in clusters (Oemler 1974;

* crwheele@uci.edu

Dressler 1980). This, and the fact that both dSphs and dIrrs can be fit with exponential light profiles (Mateo 1998; Ferguson & Binggeli 1994; Faber & Lin 1983), is often used to argue in favor of a dwarf irregular transformation-based origin for dSphs (Faber & Lin 1983; Mayer et al. 2001b). If, as is commonly understood from classical galaxy formation theory, all galaxies initially form as thin, angular momentum supported disks (White & Rees 1978; Fall & Efstathiou 1980; Blumenthal et al. 1984), then significant transformation must occur to convert these rotationally-supported galaxies into the puffy, dispersion-dominated dSphs we see today.

The currently-favored mechanism for bringing about this transformation is known as "tidal stirring" (Mayer et al. 2001a,b). According to this model, rotationally-supported dwarfs with exponential stellar disks and high gas fractions are repeatedly tidally shocked at the pericenters of their orbits. While ram pressure is primarily responsible for removing gas from the dwarf, it is the repeated tidal shocks that produce the morphological transformation. In general, for low-mass dwarfs (the majority of those found in the Local Group), this involves the creation of a tidally-induced bar, which transports high angular momentum material to the outer regions of the galaxy where it is subsequently stripped. This reduces the rotation of the system and transforms the galaxy into a spheroidal, dispersion-supported system (Mayer 2010, and references therein). In the tidal stirring model, a galaxy is generally considered to have been transformed into a dSph if it has no (or very little) gas, an ellipticity within a specific range (usually $0.1 < e < 0.5$; greater values of ellipticity indicate a more elongated shape), and if the ratio of its line-of-sight rotational velocity to its velocity dispersion, v_{rot}/σ, is below some value – usually 1, but as low as 0.5. A number of early simulations investigating this effect had considered infalling dIrr models with extremely cold disks ($v_{rot}/\sigma \simeq 5$) but more recent simulations involve somewhat hotter initial disks [1] $v_{rot}/\sigma \simeq 2 - 3$ (e.g. Kazantzidis et al. 2011a).

While tidal stirring simulations have been successful at producing systems with $v_{rot}/\sigma \lesssim 1$ (Mayer et al. 2001a,b, 2006; Klimentowski et al. 2009; Mayer 2010; Łokas, Kazantzidis & Mayer 2011; Kazantzidis et al. 2011a; Kazantzidis, Łokas & Mayer 2013; Łokas et al. 2015; Tomozeiu, Mayer & Quinn 2015), historically it has been difficult to reduce v_{rot}/σ to values < 0.5 found for many observed dwarf satellites (Mastropietro et al. 2005). The most complete transformations occur for highly eccentric orbits (Mayer et al. 2001a,b), at low inclination, and that are mildly prograde (Kazantzidis et al. 2011a; Łokas et al. 2015, but see Mayer et al. 2006). The high eccentricity in particular allows for shorter orbital times and repeated pericenter passages (typically $3 - 5$, but as many as 8). Short orbital times ($1 - 3$ Gyr) and close pericenter distances ($10 - 70$ kpc) have been shown to be particularly important to the transformation (Kazantzidis et al. 2011a). Interestingly, these simulations have often found that the accreted dIrr galaxies need to orbit within a Milky Way host potential for ~ 10 Gyr in order to be able to complete the required number of pericenter passages (Klimentowski et al. 2009; Mayer 2010; Łokas, Kazantzidis & Mayer 2011; Kazantzidis et al. 2011a; Kazantzidis, Łokas & Mayer 2013; Łokas et al. 2015; Tomozeiu, Mayer & Quinn 2015).

One major issue with any scenario that requires ~ 10 Gyr in order to transform a dIrr to a dSph is that this is quite long compared

to the expected accretion times for satellites derived from cosmological simulations of Milky Way and Local Group analogues. Specifically, the overwhelming majority of Milky Way satellites are predicted to have fallen in less than 10 Gyr ago (Rocha, Peter & Bullock 2012; Garrison-Kimmel et al. 2014; Fillingham et al. 2015; Wetzel, Deason & Garrison-Kimmel 2015), with $\sim 40\%$ accreted within the last 4 Gyr. Only 2 of the 11 classical Milky Way dwarf satellites are dIrrs (which appear to have fallen in very recently, Besla et al. 2007), and they are significantly more massive than the dSph satellites. This suggests that any environmental transformation associated with dSph formation needs to occur within ~ 2 Gyr of accretion (Fillingham et al. 2015; Wetzel, Deason & Garrison-Kimmel 2015). Furthermore, at least two dSphs, Cetus and Tucana, currently exist at large distances from either the Milky Way or Andromeda (681 and 882 kpc from the closest giant, McConnachie 2012). They, like the dSphs much closer to their hosts, have little to no gas and their stars are dispersion rather than rotationally-supported (see below). Explaining the existence of such distant objects as the result of tidal stirring poses a particularly difficult challenge to the model. Due to this difficulty, Kazantzidis et al. (2011a) predict that distant dSphs should have systematically higher values of v_{rot}/σ. Alternatively, it has been shown that dwarfs with highly cored dark-matter profiles undergo faster transformations (after just $1 - 2$ pericenter passages, Kazantzidis, Łokas & Mayer 2013; Tomozeiu, Mayer & Quinn 2015). This reduction in required time spent near the host would be particularly useful in explaining the lack of rotation in an object like Leo I, which has undergone only a single pericenter passage at a distance of ~ 100 kpc from the Milky Way (Sohn et al. 2013; Boylan-Kolchin et al. 2013).

There are other alternative mechanisms for transforming a dIrr into a dSph that require the initial galaxy to interact with another object. Dwarf-dwarf mergers can create dSphs (Moore et al. 1996; Kazantzidis et al. 2011b), and the mechanism is satisfyingly similar to models proposed for transforming massive disks into giant ellipticals (Icke 1985). Starkenburg, Helmi & Sales (2015) propose that the spheroidal shapes of dSphs can be reproduced by mergers between dwarf galaxies and lower-mass dark halos, but do not discuss rotation support. Another model, "resonant stripping", posits that a fly-by between a dwarf and a galaxy 100 times its mass can instigate resonances in the smaller dwarf that preferentially strip the stellar material (D'Onghia et al. 2009). Interactions between dwarfs in the Local Group are common (Deason et al. 2014), but merger-based transformation scenarios fail to explain the "Local Group morphology-density relation," and so are not likely to account for a large fraction of observed dSphs.

Given the strict requirements for the tidal stirring mechanism to be effective, it seems reasonable to question the initial conditions used for dwarf galaxies in these models. The traditional picture of disk galaxy formation was developed for massive galaxies (Fall & Efstathiou 1980; Blumenthal et al. 1984) with virial temperatures $T_v \sim 10^6$ K, which is well above the expected bulk ISM temperature of a cooled gas in a galaxy $T_g \sim 10^4$ K. In this case, the pressure support radius of cooled gas will be tiny compared to the angular-momentum support radius. [2] It is in this sense

---

[1] Kazantzidis, Łokas & Mayer (2013) suggest that if dark matter halos are more core-like, then it would be natural to consider $v_{rot}/\sigma \simeq 1 - 1.5$ as starting points because v_{rot} is reduced at small radii while σ might be expected to stay fixed.

[2] The radius of pressure support declines exponentially as the ratio T_g/T_v shrinks, where T_g is a phenomenological proxy that mimics the net effect of velocity dispersion from various feedback effects, such as inefficient cooling, heating by an internal or external ultraviolet (UV) background, supernova feedback, turbulent pressure, or cosmic-ray heating, among others (Kaufmann, Wheeler & Bullock 2007).

that the disk of a massive galaxy is expected to be "cold." However, Kaufmann, Wheeler & Bullock (2007, hereafter KWB) show, using a simple analytic approximation and hydrodynamic simulations, that low-mass galaxies with shallow potential wells and modest virial temperatures ($T_v \lesssim 10\,T_g$) will tend to have pressure support radii that are comparable to their angular-momentum support radii. KWB did not look at v_{rot}/σ explicitly, but showed that at low virial mass ($M_{vir} \lesssim 10^{11}\,M_\odot$), the dispersion-supported component of a galaxy should begin to rival the rotationally-supported component. The above arguments only strengthen if one considers additional ISM pressure imparted on small galaxies from internal feedback effects and turbulent motions. Moreover, stars, unlike gas, can never re-cool after their orbits are disturbed by potential fluctuations or mergers. Taken together, these arguments suggest that the stellar populations of dwarf galaxies residing in the field are not necessarily expected to exhibit well-ordered, disk-like motions as seen in their larger cousins.

Recently, large samples of stellar kinematic data for local dIrr galaxies have become available (Simon & Geha 2007; Fraternali et al. 2009; Leaman et al. 2009, 2012; Kirby et al. 2014). These data enable more detailed studies of the pressure support in field dwarfs. In particular, Kirby et al. (2014) present a stellar kinematic analysis of seven (non-satellite) dwarf galaxies in the local volume, and showed that only one among them (Pegasus) demonstrates a clear sign of rotation in its stellar population. While they did not explicitly rule out rotation in the other objects, the work of Kirby et al. provides some suggestion that a high degree of rotation support is not the rule among isolated dwarfs.

In what follows, we conduct a systematic search for stellar rotation in Local Group dwarfs. We use a Bayesian analysis on a large observational sample of dwarfs consisting of twenty eight MW and M31 dSphs, two dwarf ellipticals (dEs), and ten dwarfs beyond the virial radii of either the MW or M31 (including two isolated dSphs and eight dIrrs) to estimate v_{rot}/σ. We confirm previous findings that both the MW and M31 dSphs, with few exceptions, have stellar populations that are not rotating. We show further that isolated dwarfs in the Local Group are also primarily dispersion-supported, with only one of eight showing strong Bayesian evidence for rotation, and two having weak to inconclusive Bayesian evidence. We propose an alternative formation scenario for dSphs galaxies: most dwarf galaxies form initially as puffy, dispersion-supported or slowly rotating systems, and gas removal via ram pressure stripping (enabled by internal feedback) is likely the main process that leads to the formation of dSphs. We demonstrate the feasibility of this in a ΛCDM scenario by using the same Bayesian analysis to measure the rotation support in four hydrodynamic cosmological zoom-in simulations of *isolated* dwarf galaxies run with FIRE/GIZMO. The star particles in our simulated isolated dwarf galaxies are dispersion-supported, without any interaction with a more massive galaxy, and their ellipticities are also similar to the known dSph population without the need for harassment.

In Section 2, we highlight our observational sample. Our simulated dwarfs and their characteristics are described in Section 3. Section 4.1 is used to explain the Bayesian analysis we perform on each galaxy. The results of our systematic search for stellar rotation are given in Section 5. We discuss these findings in Section 6 and conclude in Section 7.

2 OBSERVATIONS

We analyze spectroscopic data for 40 Local Group galaxies, which are listed by name in Table 1 (column 1) along with the number of stars used in our analysis (column 10). We use measured line-of-sight velocities for each star as well as the associated errors kindly provided by the authors in the references listed below.

Among Milky Way satellites, our sample includes all nine of the classical dwarfs: Carina, Fornax, Sculptor, Sextans (Walker et al. 2009), Draco (Walker, Olszewski & Mateo 2015), Leo I (Mateo, Olszewski & Walker 2008), Leo II (Koch et al. 2007a), Sagittarius (Frinchaboy et al. 2012), and Ursa Minor (Pace 2015, in prep.). For the ultra-faint dSphs of the Milky Way we examine Canes Venatici I, Canes Venatici II, Coma Berenices, Hercules, Leo IV, Ursa Major I, Ursa Major II (Simon & Geha 2007), and Boötes I (Koposov et al. 2011).

For the M31 system we examine 14 satellites: And II (Ho et al. 2012), And I, And III, And V, And VII, And IX, And X, And XIII, And XIV, And XV, (Tollerud et al. 2012), And VI, (Collins et al. 2013) Cassiopeia 3, and Lacerta 1 (Martin et al. 2014), NGC 147, and NGC 185 (Geha et al. 2010).

Finally, we study ten isolated Local Group galaxies: Tucana (Fraternali et al. 2009), Leo T (Simon & Geha 2007), NGC 6822, IC 1613, VV 124, Pegasus dIrr, Leo A, Cetus and Aquarius (Kirby et al. 2014), and WLM (Leaman et al. 2009, 2012). The dwarf galaxies Phoenix (Irwin & Tolstoy 2002) and Antlia (Tolstoy & Irwin 2000) have spectroscopic samples that are too small to search for rotation.

All samples are homogeneous except for WLM, which consists of data from two distinct observations (one with Keck and the other with the VLT). The analysis includes all stars in each sample, and the samples span varying degrees of spatial extent within the galaxy (the majority go out to ∼ 2 effective radii). All stars analyzed are either red giant or horizontal branch stars.

A subset of our analysis includes an allowance for proper motion (see below). This effect is only important for the satellites of the Milky Way. We specifically use proper motion measurements from *Hubble Space Telescope* (HST) observations when available. In the standard frame (μ_α, μ_δ) and in units of mas century^{-1}, these are: Carina ($22 \pm 9, 15 \pm 9$; Piatek et al. 2003), Draco ($17.7 \pm 6.3, -22.1 \pm 6.3$; Pryor, Piatek & Olszewski 2015), Fornax ($47.6 \pm -4.6, -36.0 \pm 4.1$; Piatek et al. 2007), Leo I ($11.40 \pm 2.95, -12.56 \pm 2.93$; Sohn et al. 2013), Leo II ($10.4 \pm 11.3, -3.3 \pm 15.1$; Lépine et al. 2011), Sagittarius ($-254 \pm 18, -119 \pm 16$; Massari et al. 2013), Sculptor ($9 \pm 13, 2 \pm 13$; Piatek et al. 2006), and Ursa Minor ($-50 \pm 17, 22 \pm 16$; Piatek et al. 2005).

3 SIMULATIONS

Our simulations were previously presented in Wheeler et al. (2015), and consist of four[3] cosmological zoom-in simulations of isolated dwarf galaxy halos. Two were run at the mass of the halos believed to host classical dwarf galaxies ($M_{vir} \simeq 10^{10}\,M_\odot$) and two at lower

---

[3] In Wheeler et al. (2015), we also analyzed two additional simulations that used the same initial conditions as one of our ∼ 10^10 M_⊙ halos, but were run with slight changes to the subgrid feedback implementation (see Wheeler et al. 2015 for details). We have not included analysis of those two runs in the text or in the figures here, but note that they have values of v_{rot}/σ and ellipticity similar to the other runs analyzed here, and so would not change our results if included.

Dwarf	Category	$M_\star(10^6\,\mathrm{M_\odot})$	$d_{\mathrm{MW/M31}}$ (kpc)	ellipticity	v_{rot}/σ	v_{rot} (km s^{-1})	σ (km s^{-1})	N_{stars}	ln B	Reference
Coma Berenecis	UF dSph	0.0037	45	$0.38^{0.14}_{-0.14}$	$0.45^{0.51}_{-0.66}$	$2.09^{2.09}_{-3.10}$	$4.60^{0.95}_{-0.83}$	59	-2.44	(a), (b)
Ursa Major II	UF dSph	0.0041	38	$0.63^{0.05}_{-0.05}$	$0.51^{0.51}_{-0.57}$	$3.40^{3.89}_{-2.97}$	$6.81^{1.91}_{-1.51}$	20	-1.68	(a), (b)
Canis Venatici II	UF dSph	0.0079	161	$0.52^{0.11}_{-0.11}$	$0.38^{0.42}_{-0.43}$	$1.84^{1.94}_{-2.12}$	$4.96^{1.35}_{-1.07}$	25	-2.58	(a), (b)
Ursa Major I	UF dSph	0.014	102	$0.80^{0.04}_{-0.04}$	$0.11^{0.33}_{-0.30}$	$0.87^{2.68}_{-2.43}$	$7.95^{1.22}_{-1.02}$	39	-2.80	(a), (b)
Bootes I	UF dSph	0.029	64	$0.39^{0.06}_{-0.06}$	$0.19^{0.20}_{-0.21}$	$1.00^{1.11}_{-1.00}$	$5.17^{0.56}_{-0.48}$	74	-3.18	(a), (c)
Hercules	UF dSph	0.037	126	$0.68^{0.08}_{-0.08}$	$0.09^{0.37}_{-0.34}$	$0.51^{1.89}_{-2.03}$	$5.55^{1.16}_{-0.93}$	30	-3.14	(a), (c)
Canis Venatici I	UF dSph	0.23	218	$0.39^{0.03}_{-0.03}$	$0.01^{0.11}_{-0.12}$	$0.05^{0.88}_{-0.92}$	$7.69^{0.48}_{-0.45}$	214	-3.86	(a), (c)
Draco	MW dSph	0.29	76	$0.31^{0.02}_{-0.02}$	$0.18^{0.07}_{-0.07}$	$1.66^{0.60}_{-0.59}$	$9.06^{0.31}_{-0.28}$	476	-0.54	(a), (d)
Ursa Minor	MW dSph	0.29	78	$0.56^{0.05}_{-0.05}$	$0.13^{0.09}_{-0.10}$	$1.07^{0.81}_{-0.68}$	$7.99^{0.24}_{-0.24}$	867	-2.70	(a), (e)
Carina	MW dSph	0.38	107	$0.33^{0.05}_{-0.05}$	$0.03^{0.06}_{-0.06}$	$0.20^{0.40}_{-0.42}$	$6.44^{0.20}_{-0.21}$	758	-4.44	(a), (f)
Sextans	MW dSph	0.44	89	$0.35^{0.05}_{-0.05}$	$0.05^{0.08}_{-0.10}$	$0.33^{0.61}_{-0.67}$	$7.10^{0.29}_{-0.28}$	424	-4.07	(a), (f)
Leo II	MW dSph	0.74	236	$0.13^{0.05}_{-0.05}$	$0.01^{0.17}_{-0.18}$	$0.04^{1.23}_{-1.17}$	$6.77^{0.49}_{-0.44}$	164	-3.41	(a), (g)
Sculptor	MW dSph	2.3	86	$0.32^{0.03}_{-0.03}$	$0.05^{0.05}_{-0.05}$	$0.42^{0.45}_{-0.43}$	$8.80^{0.19}_{-0.18}$	1349	-4.07	(a), (f)
Sagittarius*	MW dSph	3.5	18	$0.64^{0.02}_{-0.02}$	$0.42^{0.05}_{-0.05}$	$6.22^{0.77}_{-0.75}$	$14.86^{0.32}_{-0.30}$	1310	28.82	(a), (h)
Leo I	MW dSph	5.5	258	$0.21^{0.03}_{-0.03}$	$0.02^{0.10}_{-0.11}$	$0.19^{0.94}_{-0.98}$	$9.02^{0.39}_{-0.37}$	327	-3.53	(a), (i)
Fornax	MW dSph	20	149	$0.30^{0.01}_{-0.01}$	$0.02^{0.04}_{-0.05}$	$0.23^{0.42}_{-0.55}$	$10.59^{0.16}_{-0.16}$	2409	-4.08	(a), (f)
Andromeda XIV	M31 dSph	0.02	162	$0.20^{0.11}_{-0.11}$	$0.29^{0.36}_{-0.37}$	$1.78^{2.25}_{-2.03}$	$5.98^{1.09}_{-0.92}$	48	-2.53	(a), (j), (k)
Andromeda X	M31 dSph	0.096	110	$0.30^{0.18}_{-0.18}$	$0.17^{0.44}_{-0.43}$	$1.23^{3.19}_{-3.06}$	$7.20^{2.14}_{-1.58}$	21	-2.52	(a), (j), (k)
Andromeda IX	M31 dSph	0.15	40	$0.12^{0.07}_{-0.07}$	$0.05^{0.40}_{-0.36}$	$0.65^{4.75}_{-4.46}$	$12.13^{2.50}_{-2.02}$	32	-2.21	(a), (j), (k)
Andromeda V	M31 dSph	0.39	110	$0.28^{0.07}_{-0.07}$	$0.03^{0.25}_{-0.29}$	$0.29^{3.28}_{-2.78}$	$11.09^{1.25}_{-1.10}$	85	-2.53	(a), (j), (k)
Andromeda XV	M31 dSph	0.49	174	$0.24^{0.10}_{-0.10}$	$0.26^{0.51}_{-0.47}$	$1.30^{2.41}_{-2.25}$	$5.03^{1.63}_{-1.34}$	29	-2.69	(a), (j), (k)
Andromeda III	M31 dSph	0.83	75	$0.59^{0.03}_{-0.03}$	$0.69^{0.44}_{-0.66}$	$6.45^{6.10}_{-3.83}$	$9.40^{1.58}_{-1.32}$	62	0.66	(a), (j), (k)
Andromeda VI	M31 dSph	2.8	269	$0.41^{0.03}_{-0.03}$	$0.19^{0.40}_{-0.39}$	$2.52^{5.26}_{-5.26}$	$13.25^{2.68}_{-2.16}$	38	-1.91	(a), (j), (l)
Andromeda I	M31 dSph	3.9	58	$0.29^{0.03}_{-0.03}$	$0.13^{0.64}_{-0.76}$	$1.55^{6.96}_{-8.38}$	$11.03^{2.30}_{-1.85}$	51	-1.20	(a), (j), (k)
Cassiopeia III	M31 dSph	3.98	144	$0.50^{0.09}_{-0.09}$	$0.11^{0.16}_{-0.13}$	$0.92^{1.11}_{-1.33}$	$8.33^{0.56}_{-0.52}$	212	-3.36	(m), (n)
Lacerta I	M31 dSph	6.3	275	$0.43^{0.07}_{-0.07}$	$0.11^{0.18}_{-0.17}$	$1.15^{1.77}_{-1.84}$	$10.32^{0.83}_{-]0.75}$	127	-2.97	(m), (n)
Andromeda II	M31 dSph	7.6	184	$0.14^{0.02}_{-0.02}$	$1.09^{0.10}_{-0.10}$	$8.87^{0.70}_{-0.69}$	$8.17^{0.39}_{-0.38}$	474	63.33	(a), (j), (o)
Andromeda VII	M31 dSph	9.5	218	$0.13^{0.04}_{-0.04}$	$0.33^{0.15}_{-0.15}$	$4.38^{1.88}_{-1.95}$	$13.12^{1.08}_{-1.00}$	135	-0.51	(a), (j), (k)
NGC 147	dE/dSph	62	142	$0.46^{0.02}_{-0.02}$	$0.65^{0.06}_{-0.06}$	$11.77^{0.95}_{-0.96}$	$18.14^{0.64}_{-0.62}$	520	66.14	(a), (j), (p)
NGC 185	dE/dSph	187	442	$0.22^{0.01}_{-0.01}$	$0.31^{0.06}_{-0.06}$	$7.41^{1.43}_{-1.45}$	$23.91^{0.88}_{-0.83}$	442	8.86	(a), (j), (p)
Leo T	Iso dIrr/dSph	0.14	422	$0.29^{0.12}_{-0.14}$	$0.01^{0.42}_{-0.44}$	$0.11^{3.76}_{-3.64}$	$8.53^{2.16}_{-1.63}$	19	-2.44	(a), (b)
Tucana	Iso dSph	0.56	882	$0.48^{0.03}_{-0.03}$	$0.34^{0.4}_{-0.53}$	$7.31^{9.74}_{-11.53}$	$21.17^{4.88}_{-3.47}$	19	-0.96	(a), (q)
Aquarius	Iso dIrr/dSph	1.6	1066	$0.50^{0.10}_{-0.10}$	$1.99^{0.83}_{-0.76}$	$10.93^{3.03}_{-3.37}$	$5.51^{1.42}_{-1.12}$	43	1.61	(a), (r)
Cetus	Iso dSph	2.6	681	$0.33^{0.06}_{-0.06}$	$0.08^{0.18}_{-0.21}$	$0.66^{1.45}_{-1.73}$	$8.30^{0.83}_{-0.76}$	120	-3.19	(a), (r)
Leo A	Iso dIrr	6.0	803	$0.40^{0.03}_{-0.03}$	$1.64^{0.68}_{-0.61}$	$8.68^{2.73}_{-2.68}$	$5.31^{1.09}_{-0.94}$	50	1.23	(a), (r)
Pegasus	Iso dIrr	6.61	474	$0.46^{0.02}_{-0.02}$	$1.29^{0.20}_{-0.19}$	$14.67^{1.97}_{-1.82}$	$11.36^{0.93}_{-0.83}$	105	28.90	(a), (r)
VV 124	Iso dIrr/dSph	8.3	1367	$0.44^{0.04}_{-0.04}$	$0.41^{0.34}_{-0.31}$	$3.86^{3.07}_{-2.89}$	$9.28^{1.09}_{-0.94}$	87	-1.88	(a), (r)
WLM	Iso dIrr	43	836	$0.65^{0.01}_{-0.01}$	$0.56^{0.11}_{-0.10}$	$8.73^{1.57}_{-1.53}$	$15.58^{0.95}_{-0.86}$	180	10.53	(a), (s), (t)
IC 1613	Iso dIrr	100	517	$0.24^{0.06}_{-0.06}$	$0.03^{0.23}_{-0.29}$	$0.32^{2.40}_{-3.13}$	$10.71^{0.81}_{-0.72}$	143	-2.43	(i), (r)
NGC 6822	Iso dIrr	100	452	$0.24^{0.05}_{-0.05}$	$0.39^{0.11}_{-0.12}$	$8.78^{2.46}_{-2.75}$	$22.57^{1.02}_{-0.94}$	314	3.47	(a), (r)

Table 1. Properties and estimated parameters of all galaxies in the observed sample. (1) Name of galaxy. (2) Galaxy type. (3) Galaxy stellar mass from literature. (4) Distance from galaxy to its nearest massive neighbor from literature – either the Milky Way or M31. (5) Ellipticity of galaxy obtained from literature, with error. (6) Median of parameter v_{rot}/σ from Bayesian analysis, with $\pm 1\ \sigma$ error. (7) Median rotational velocity from Bayesian analysis, with $\pm 1\ \sigma$ error. (8) Median velocity dispersion from Bayesian analysis, with $\pm 1\ \sigma$ error. (9) Number of stars used in analysis. (10) ln B, where B is the Bayes factor. Values less than 3 imply weak/inconclusive evidence for rotation and negative values favor non-rotation to varying degrees, see Section 4.1 for details). (11) Citations: a) McConnachie 2012, b) Simon & Geha 2007 c) Koposov et al. 2011, d) Walker, Olszewski & Mateo 2015, e) Pace 2015, in prep., f) Walker et al. 2009, g) Koch et al. 2007a, h) Frinchaboy et al. 2012, i) Mateo 1998, j) Salomon et al. 2015, k) Tollerud et al. 2012, l) Collins et al. 2013, m) Martin et al. 2013, n) Martin et al. 2014, o) Ho et al. 2012, p) Geha et al. 2010, q) Fraternali et al. 2009, r) Kirby et al. 2014, s) Leaman et al. 2009, t) Leaman et al. 2012. *We exclude Sagittarius from all figures. See Section 4.2 for details.

mass ($M_{\rm vir} \simeq 10^9 \, {\rm M}_\odot$) (see Wheeler et al. 2015 for details). All of our simulations were run with the fully conservative cosmological hydrodynamic code Gizmo (Hopkins et al. 2014) in PSPH-mode, with the standard FIRE feedback implementation. Every run uses a gas particle mass of $m_p^{\rm gas} = 255 \, {\rm M}_\odot$ except for UFD 2, which uses $m_p^{\rm min} = 499 \, {\rm M}_\odot$. The gas force resolution varies from $\epsilon_{\rm gas}^{\rm min} = 1.0 - 2.8$ pc, and the stellar masses of the resultant galaxies span $\sim 10^{3.9} - 10^{6.3} \, {\rm M}_\odot$.

All of these cosmological simulations are of isolated dwarfs, that is, with no large neighbors in either the high or low resolution regions. All but one of the ($M_{\rm vir} \simeq 10^9 \, {\rm M}_\odot$) dwarfs were selected from 5 h^{-1} Mpc boxes to have typical values of spin parameter λ, concentration, and formation time for their mass range, and also to have small Lagrangian volumes (Oñorbe et al. 2014). The lowest mass ($M_{\rm vir} \simeq 10^9 \, {\rm M}_\odot$) dwarf was selected from a 25 h^{-1} Mpc box and required to have no other halos of 50% or more of its mass within 4 $R_{\rm vir}$ at $z = 0$ and a small Lagrangian volume. All analysis was performed on the $z = 0$ snapshot of each simulation.

4 MEASURING ROTATION

4.1 Bayesian Analysis

For each galaxy, we investigate a model with and without rotation in order to determine if there is evidence in favor of rotation. We do not assume the stellar components necessarily exist within coherently rotating disks – the rotation we measure is based entirely on the observed gradient in coherent velocity across the face of the galaxy in the sky. We assume that the likelihood of observing a distribution $\mathcal{D} = (\mathbf{v}, \epsilon)$ of N stars with line-of-sight velocities v_j and associated errors ϵ_j is:

$$\mathscr{L} = \prod_{j=1}^{N} \frac{1}{\sqrt{2\pi(\sigma^2 + \epsilon_j^2)}} \exp\left[-\frac{1}{2}\frac{(v_j - v_j^{\rm rel})^2}{\sigma^2 + \epsilon_j^2}\right], \qquad (1)$$

where σ is the underlying (constant) velocity dispersion and $v_j^{\rm rel}$ is a relative velocity, the form of which depends on whether the model is rotating or non-rotating. In the absence of rotation, the relative velocity is simply the average bulk motion of the system $v_j^{\rm rel} = \bar{v}$. With rotation, the relative velocity becomes

$$v_j^{\rm rel} = \bar{v} + v_{\rm rot} \cos(\theta - \theta_j), \qquad (2)$$

where θ is a model parameter (measured from North to East) that defines the axis of rotation, θ_j is the position angle for each star, and $v_{\rm rot}$ is the observed rotation across this axis. [4]

Note that if the galaxy's angular momentum vector is inclined relative to us with an angle i, then $v_{\rm rot} = v_o \sin i$, where v_o is the magnitude of the intrinsic rotation. In what follows we quote results for $v_{\rm rot}$ (rather than v_o) because $\sin i$ is poorly constrained for the stars. The value of $v_{\rm rot}$ is a lower limit on the intrinsic value of v_o. However, as can be seen in Table 1, there is a small amount of scatter in the $v_{\rm rot}$ values calculated, despite the very large sample.

For nearby dwarfs, the line-of-sight velocities as measured from Earth will not project along parallel directions. One implication is that if a galaxy is moving in the transverse direction, a significant component of this proper motion can be observed as a gradient in the line-of-sight motions of stars across the face of

the galaxy (Feast, Thackeray & Wesselink 1961; van der Marel et al. 2002). This perspective proper motion effect can be important for interpreting the dynamics of local galaxies (Kaplinghat & Strigari 2008; Walker, Mateo & Olszewski 2008) and we therefore include it when possible here. All classical dSphs except Sextans have proper motion measurements from Hubble Space Telescope (HST) observations. For these galaxies, we include the perspective proper motion effects on the relative velocity as $v_{\rm rel} \rightarrow v_{\rm rel} + v_{\rm perspec}$, marginalizing over the proper motion using Gaussian priors centered on the reported measurements (see below). We do not include the (currently unmeasured) proper motion parameters in Sextans or any of the Ultra Faint dSphs. The isolated and the M31 systems are too distant for proper motions to have a measurable effect.

The posterior distribution, $\mathcal{P}(\mathcal{M}|\mathcal{D}, H)$, is the distribution of model parameters $\mathcal{M}$ given the observation of data $\mathcal{D}$. The symbol H represents the model under consideration: we consider both rotating and non-rotating scenarios. The likelihood, $\mathscr{L} = \mathcal{P}(\mathcal{D}|\mathcal{M}, H)$, is the probability to observe the data given a set of model parameters. The posterior is related to the likelihood via Bayes' Theorem:

$$\mathcal{P}(\mathcal{M}|\mathcal{D}, H) = \frac{\mathcal{P}(\mathcal{D}|\mathcal{M}, H) Pr(\mathcal{M})}{\mathcal{P}(\mathcal{D}, H)}, \qquad (3)$$

where $Pr(\mathcal{M})$ is the prior distribution, set by our preconceived knowledge of the model. In our fiducial case that explores rotation and allows for proper motion, we have model parameters $\mathcal{M} = (\bar{v}, \sigma, v_{\rm rot}, \theta, \mu_\alpha, \mu_\delta)$, where μ_α and μ_δ are the proper motions.

The denominator in Equation 3, $Z = \mathcal{P}(\mathcal{D}, H)$, is referred to as the Bayesian evidence. It is a normalization factor that is commonly ignored, but will be used for model comparison in our analysis. To test whether the rotating model is favored, we compute the natural log of the Bayes factor, which is defined as the ratio of evidence for each model: $\ln B = \ln(Z_{\rm rotating}/Z_{\rm non-rotating})$. A value greater than zero favors the rotation model. The significance of the rotation is based on its magnitude on Jeffery's scale: (0-1), (1-3), (3-5), (5+), corresponds to inconclusive, weak, moderate, and strong evidence in favor of the rotating model. Likewise, the corresponding negative values offer varying degrees of evidence in favor of the non-rotating model. The natural log of the Bayes factor for each galaxy in this work can be found in column 10 of Table 1.

We compute the posterior distribution with a Multi-Nested Sampling routine (Feroz & Hobson 2008; Feroz, Hobson & Bridges 2009). This method directly calculates the evidence and, as a by-product, samples the posterior distribution (for a review of Bayesian method and model comparison see Trotta 2008). We marginalize over the prior ranges: $-20 < \bar{v} - v_{\rm g} < +20 \, {\rm km \, s^{-1}}$, $0 < \sigma < +75 \, {\rm km \, s^{-1}}$, $-50 < v_{\rm rot} < +50 \, {\rm km \, s^{-1}}$, $0 < \theta < +\pi$, $-300 < \mu_\alpha - \bar{\mu}_{\alpha,{\rm HST}} < +300 \, {\rm mas \, century^{-1}}$, and $-300 < \mu_\delta - \bar{\mu}_{\delta,{\rm HST}} < +300 \, {\rm mas \, century^{-1}}$, where $v_{\rm g}$, $\bar{\mu}_{\alpha,{\rm HST}}$, and $\bar{\mu}_{\delta,{\rm HST}}$ are the values for each galaxy taken from the literature. For several galaxies, we examine larger ranges of $\bar{v}$, μ_α, and μ_α. This is significant only for Sagittarius, where its close position causes its best fit HST proper motions to be well outside the range considered for other dwarfs. For galaxies with rotation axes near 0 or π, we marginalize over $-\pi/2 < \theta < +\pi/2$. All priors are uniform except μ_α and μ_δ, which are Gaussian and centered on the HST measurements. We test our method with mock data sets and verify that the input parameters are recovered.

Properties taken from the literature and parameter estimates for each observed galaxy in our analysis, given observational dataset $D(v_j, \epsilon_j, \theta_j)$ for each star, can be found in Table 1. Before

---

[4] Note that we do not explore radially-varying rotation curves, and thus are effectively measuring the *average* rotation of the stars in the sample.

moving on to our broad results (Section 5) we will first comment on several galaxies of particular interest in comparison to past work in the literature.

4.2   Comments on Individual Galaxies

Sagittarius: Peñarrubia et al. (2010) predict significant rotation in this galaxy based on simulations aimed at reproducing the Sagittarius (Sgr) stream. However, in their work they assumed the progenitor of Sgr was a late-type disk galaxy ($v_{rot} \approx 20$ km s^{-1}). Follow-up work by Peñarrubia et al. (2011) did not detect rotation of this magnitude and could only reproduce the line-of-sight velocities observed today using progenitor models with no or little rotation. Similar searches for rotation in Sagittarius have made no conclusive detection (Ibata et al. 1997; Frinchaboy et al. 2012).

Our result suggests some mild rotation ($v_{rot}/\sigma \simeq 0.64$; $\ln(B) = 28.8$) but this determination is complicated by the large field of view occupied by Sagittarius on the sky. There are three different proper motion measurements (Dinescu et al. 2005; Pryor, Piatek & Olszewski 2010; Massari et al. 2013). All three are discrepant and were obtained from analyzing different fields within Sagittarius. It is possible that the discrepancy is due to the 3D perspective motion or the internal motions of stars within the galaxy. In our fiducial analysis we use the result of Massari et al. (2013): $-254\pm18, -119\pm16$ in mas century^{-1}. However, these same authors also transform each of the three measurements into the center of mass frame and perform a weighted average to obtain a significantly different value: $(-301 \pm 11, -145 \pm 11)$. Using this latter proper motion, we find less rotational support $v_{rot}/\sigma = 0.42 \pm 0.05$.

The kinematic axis preferred in our analysis is $\theta = -69 \pm 3°$, which is offset from the photometric major axis of $\theta = 102 \pm 2°$ (McConnachie 2012). A velocity gradient along the major axis is expected based on the 3D motion of Sagittarius (Peñarrubia et al. 2011; Frinchaboy et al. 2012). It is peculiar, then, that our model favors attributing part of the gradient to rotation instead of the perspective motion. Part of the signal could be induced by tidal interactions, but a more in-depth analysis of the Sagittarius system is required to make a strong conclusion. Another origin of this problem could be the fact that we are not including a Milky Way model to deal with contamination in our sample. We distrust our v_{rot}/σ analysis for these reasons, and exclude Sagittarius from all figures. However, we note that our estimated value suggests that Sagittarius is not rotationally-supported, and it would lie in the same general region as the rest of the dSphs analyzed in this work.

NGC 6822: We find moderate evidence for stellar rotation in RGB stars in this galaxy ($\ln B = 3.47$) but the rotation is sub-dominant to the velocity dispersion with $v_{rot}/\sigma = 0.39$. The rotation axis is offset from the photometric position angle (located at $\theta = 65°$, Battinelli, Demers & Kunkel 2006) by $\approx 135°$: $v_{rot} = 8.8^{+2.5}_{-2.8}$ km s^{-1}, $\theta = -70^{+13}_{-10}$, $\sigma = 22.6^{+1.0}_{-0.9}$. Stellar rotation in Carbon stars was previously detected along the major axis (Demers, Battinelli & Kunkel 2006). As the HI disk is perpendicular to the stellar component, they label NGC 6822 as a polar ring galaxy. N-type Carbon stars have variable velocity, limiting the precision of the Demers, Battinelli & Kunkel (2006) measurements to ± 15 km s^{-1}. In addition, their sample was created from two telescopes, with a velocity offset of 46 km s^{-1} between each measurement and $\Delta \bar{v} \approx 20$ between the RGB stars and C stars. With these caveats, it is intriguing that the different tracers all have a different kinematic axes, possibly hinting at past mergers.

Pegasus: Stellar rotation in Pegasus was first measured in Kirby et al. (2014) with a magnitude of ~ 10 km s^{-1} across the ma-

jor axis (located at a position angle of 122°, Hunter & Elmegreen 2006). We measure a larger value that is 20° offset from the major axis: $v_{rot} = 14.7^{+2.0}_{-1.8}$, $\theta = 142.5^{+11.6}_{-9.8}$. A velocity gradient is observed in HI across the major axis. It has been suggested that this gradient could be the result of random motions (Young et al. 2003), but since the stellar rotation is detected at such high significance ($\ln B = 28.81$), it seems likely that the gas is rotating as well. This is in general agreement with the conclusions of Kirby et al. (2014).

Tucana: Fraternali et al. (2009) suggest that a flat rotation curve with $v_{rot} \approx 15$ km s^{-1} along the major axis is consistent with their data ($\theta = 97°$, Saviane, Held & Piotto 1996). Our analysis finds no evidence for rotation and prefers a value consistent with zero: $v_{rot} = -7^{+11}_{-10}$ km s^{-1} ($\ln B = -0.99$). The position angle is quite unconstrained: $\theta = -22^{+67}_{-39}$. If Tucana is rotating, a larger sample size will be required to uncover it.

And II: Ho et al. (2012) detect $v_{rot} = 8.6 \pm 1.6$ km s^{-1} along the minor axis and a maximum $v_{rot} = 10.9 \pm 2.4$ km s^{-1} located at $\theta = 113 \pm 9°$ (the photometric position angle is $\theta = 46 \pm 6°$, Ho et al. 2012). Our kinematic axis is offset from this value: $v_{rot} = 8.1 \pm 0.4$ km s^{-1}, $\theta = -28 \pm 4°$. We detect stellar rotation at strong significance near the minor axis, which could have been caused by a minor merger (Amorisco, Evans & van de Ven 2014).

WLM: We measure: $v_{rot} = 8.7 \pm 1.6$ km s^{-1}, $\sigma = 15.6 \pm 0.9$ km s^{-1}, and $\theta = 164^{16}_{-14}$. The position angle we prefer agrees well with the value of $\theta = 173°$ reported by Leaman et al. (2012). In addition, Leaman et al. (2012) measure a velocity dispersion for WLM that is broadly consistent with our value ($\sigma \approx 15$ km s^{-1}), but they report a stellar rotation that is significantly higher than our measured value (~ 15 km s^{-1}). Specifically, we measure $v_{rot}/\sigma = 0.56 \pm 0.1$ (with strong evidence), while they prefer $v_{rot}/\sigma \simeq 1$. The origin of this discrepancy is unclear. One difference in their analysis is that they infer rotation assuming that the stars are in a thin, rotating disk. We attempt a more empirically motivated model that simply measures the velocity difference across the rotation axis in the plane of the sky. While this method could potentially hide a significant amount of rotation perpendicular to the line-of-sight, it is unlikely given the high inclination angle for the galaxy ($\sim 75°$; Kepley et al. 2007). Furthermore, we apply this same analysis to every galaxy in our sample, and WLM does not seem to be an outlier.

Leaman et al. (2012) also bin their data and quote a maximum rotation for v_{rot}, obtained by a radially-varying fit. In our fiducial analysis we assume a flat rotation curve. In order to explore whether this could drive the difference, we have re-analyzed the WLM data allowing for a radially-varying rotation curve ($v_{rot} \rightarrow v_{rot} \sqrt{1 - r_o/r \arctan(r/r_o)}$ in Equation 2, where r is measured along the major axis, and r_o is the scale radius, and find that our analysis prefers both the flat rotation curve, as well as $v_{rot}/\sigma \simeq 0.5$ (marginalizing over r_o). However, more work is likely required to completely determine the origin of this discrepancy.

Leo A: Although our model prefers a fair amount of rotation in this galaxy ($v_{rot}/\sigma = 1.64^{+0.68}_{-0.61}$), our analysis yields only weak evidence for rotation in Leo A compared to a non-rotating model ($\ln B = 1.23$). There is no rotation seen in HI gas (Young & Lo 1996). Our potential rotation at $\theta \approx 34°$ is almost perpendicular to the HI disc at $\theta = 102°$. A larger kinematic sample size will be required to make a stronger statement about the rotation.

Aquarius: This galaxy has the largest preferred rotation in our sample, with $v_{rot}/\sigma \simeq 2 \pm 0.8$, though the error is large and the Bayesian evidence is weak (1.6). As with Leo A, a larger sample size will be required to make a stronger statement about the rotation and to confirm that it is indeed rotationally-supported. The kinematic axis of the HI gas is at $\theta \approx 70°$ (Begum & Chengalur

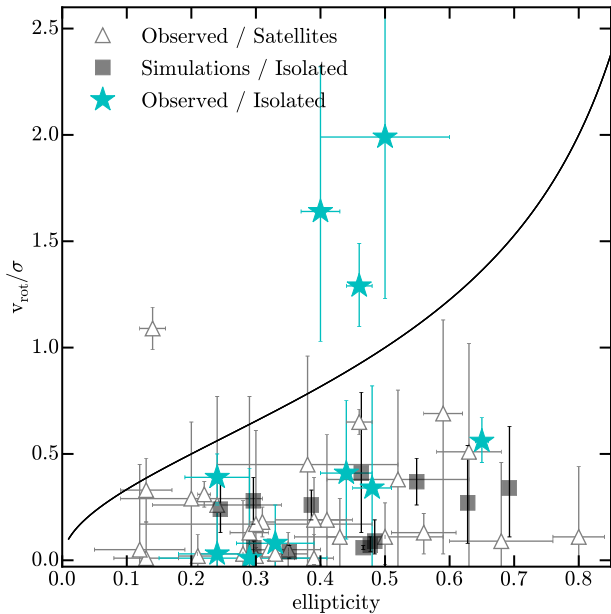**Figure 1.** Stellar rotation support $v_{\rm rot}/\sigma$ vs. e (ellipticity) for observed satellites of the Milky Way and M31 (open gray triangles), isolated Local Group Dwarfs (cyan stars), and simulated isolated (dIrr) galaxies (gray squares). The solid line shows the approximate value of $v_{\rm rot}/\sigma$ for self-gravitating objects that are flattened by rotation (Binney 1978). The four galaxies that lie above the curve are Andromeda II (open triangle), Pegasus, Leo A, and Aquarius. The majority of observed isolated dwarfs (7/10) are not rotationally supported.

Figure 2. Stellar rotation support ($v_{\rm rot}/\sigma$) vs. stellar mass for observed satellites of the Milky Way and M31 (open gray triangles), isolated Local Group Dwarfs (cyan stars), and our simulations (gray squares). No clear trend with stellar mass is seen in the data.

2004). Our kinematic axis is misaligned at $\theta \approx -5°$. The magnitude of the stellar rotation is similar to the observed gas rotation.

4.3 Simulation analysis

We apply an identical method for calculating $v_{\rm rot}/\sigma$ to the simulations (see Section 4.1). To calculate the ellipticity values for the simulations, we use a simple method outlined in Cappellari et al. (2007) for converting two dimensional field data to a single $v_{\rm rot}/\sigma$ value. For each of the three orthogonal distributions, the galaxy is rotated along the axis parallel to the line-of-sight until there is a maximum in the difference between velocity measurements in the left and right hemispheres of the projection plane. Then, after binning the stars in two dimensions, we sum up the effective "flux" in each bin and weight the bins by their distance from the center of the simulated galaxy, according to this formula:

$$(1-e)^2 = \frac{\sum_{n=1}^{N} F_n y_n}{\sum_{n=1}^{N} F_n x_n}, \qquad (4)$$

where x_n and y_n are the bin centers and we replace flux, F_n, with the number of star particles in that bin. [5] All analysis on the simulations is done on all star particles within 3 kpc of the center of each simulated galaxy. This choice allow us to select all stars that belong to the main galaxy while excluding any satellites.

[5] We have tested that this method produces ellipticity values consistent with those obtained by performing a 2D Gaussian fit to histograms of the "flux" (in this case the number of star particles) in a 2 × 2 grid along the line-of-sight to each object.
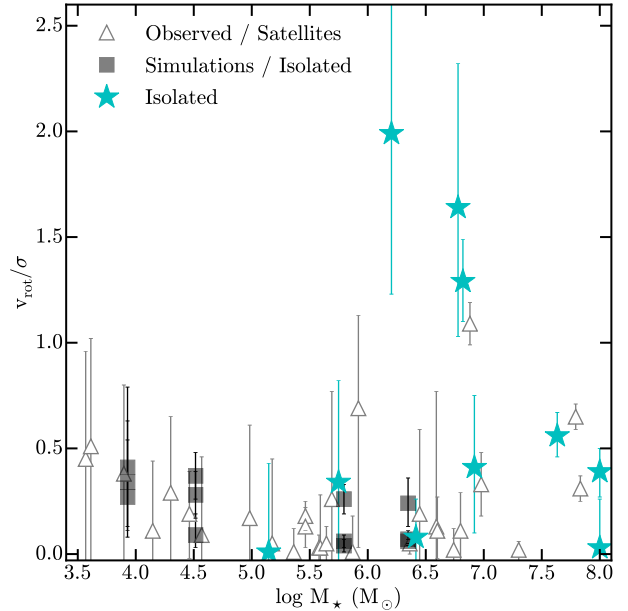
5 RESULTS

Figure 1 shows $v_{\rm rot}/\sigma$ vs. e (ellipticity) for all objects in our study. $v_{\rm rot}/\sigma$ is a standard diagnostic for detecting rotational support in more massive systems (Bender, Burstein & Faber 1993) as well. Observed Milky Way and M31 satellites are shown as open triangles, observed isolated dwarfs are shown as cyan stars, and simulated (isolated) galaxies are gray rectangles. The black line shows the expectation for self-gravitating objects flattened by rotation (Binney 1978). For the sake of concreteness, we consider objects that lie above this line to be at least marginally rotationally-supported. The galaxy ellipticity values were drawn from the literature.

Of all the galaxies in our sample, only Andromeda II, Aquarius, Leo A, and Pegasus have $v_{\rm rot}/\sigma$ values that are consistent with being supported by rotation, rather than dispersion. Of these, only And II (dSph) and Pegasus (dIrr) show rotation at strong significance. The Bayesian evidence that Aquarius and Leo A are rotating is weak; the small sample sizes prohibit a stronger statement. We also detect sub-dominant rotation at strong significance in NGC 147, NGC 185, Sagittarius, and WLM. We detect some (sub-dominant) rotation in NGC 6822, but at a lower significance.

Perhaps the most striking feature of Figure 1 is the distribution of isolated galaxies. The majority of the isolated dwarfs in our analysis have dispersion-dominated stellar populations. This is in stark contrast to the common assumption that dIrrs have stellar disks that are smaller versions of their more massive, rotating counterparts. Even the three rotation-dominated systems are only modestly so, with $v_{\rm rot}/\sigma \simeq 1.3-2$, which is significantly less rotation than a canonical cold disk, and below the values typically

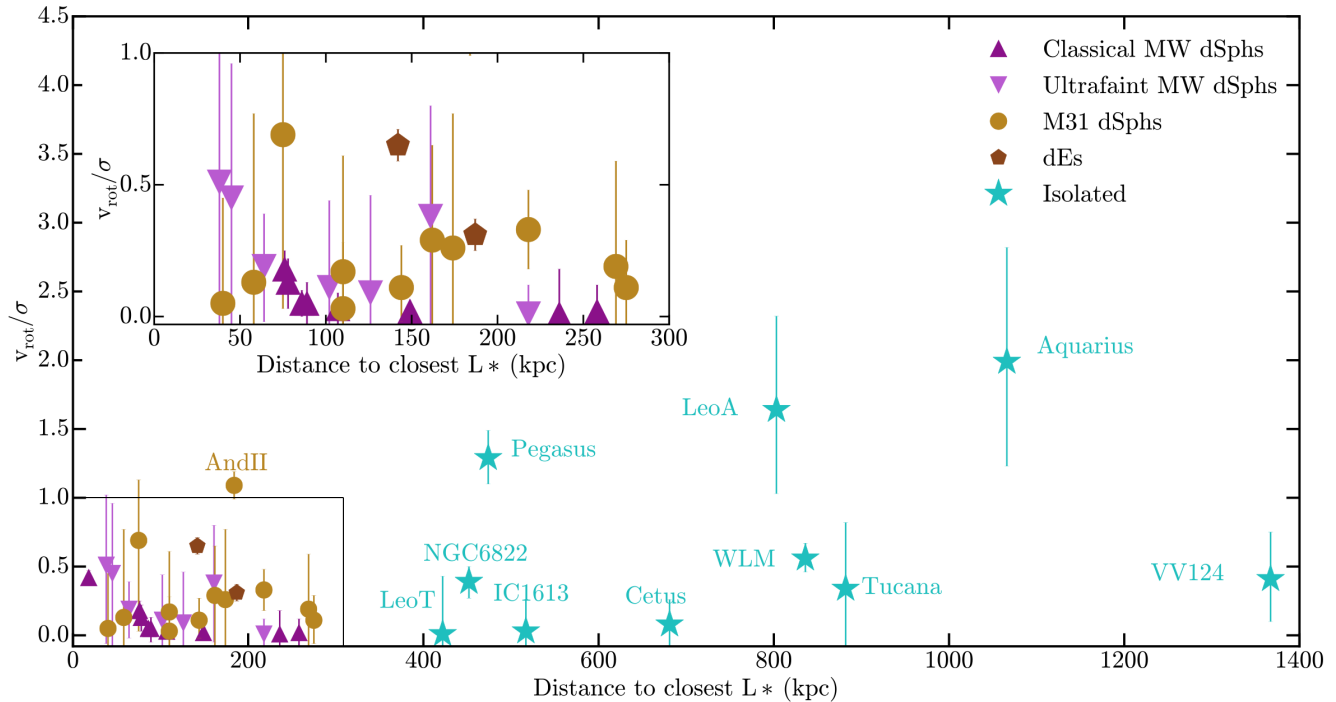**Figure 3.** Rotation support v_{rot}/σ vs $d_{MW/M31}$, distance from the dwarf to the closest $L_\star$ galaxy (either the Milky Way or M31), for observed classical Milky Way dSphs (up-facing dark magenta triangles), ultra-faint dSphs (down-facing light magenta triangles), M31 dSphs (gold circles), isolated Local Group Dwarfs (cyan stars) and dEs (brown pentagons). *Inset:* Zoomed-in region showing v_{rot}/σ vs $d_{MW/M31}$ for select (not including And II) Milky Way and M31 satellites.

assumed as initial conditions for tidal stirring scenarios for dSph formation (Kazantzidis et al. 2011a).

Our simulated dwarfs are shown as filled gray squares, each displayed at three orthogonal (but random) orientations (for a total of 12 points). The range of simulated ellipticities is consistent with the range of the observed dwarfs. Our simulated dwarfs also have v_{rot}/σ values that are broadly consistent with the data [6]. We will need more simulations (Fitts et al. 2015, in prep.) to determine whether we can ever achieve the modest fraction of isolated galaxies (3/10) with $v_{rot}/\sigma \simeq 1-2$ that we see among isolated Local Group dwarfs. If not, then this may suggest that the star formation is too bursty, or that the specific feedback implementation causes too much coupling between the injected energy and both the stellar populations and the dissipationless dark matter at the hearts of dwarf galaxies (Oñorbe et al. 2015; Chan et al. 2015).

Figure 2 shows v_{rot}/σ vs. stellar mass for all of the objects in our sample. No obvious trend with stellar mass is seen, though we note that the four systems with preferred values of $v_{rot}/\sigma > 1$ all have $M_\star > 10^6 M_\odot$. Kormendy et al. (2009) show that more luminous ($-23.24 < M_V < -15.53$) dSphs in the Virgo cluster form an extension of Local Group dSphs in the Sersic index-M_V plane, and Toloba et al. (2014) find a wide range of v_{rot}/σ values for subset of the Virgo dwarfs ($-19.0 < M_r < -16.0$), but both of these studies rely on photometry from diffuse light. Extending our analysis (using resolved stellar populations) to higher mass objects, both observed and simulated, would be useful in detecting either a trend between of v_{rot}/σ and $M_\star$ at higher mass, or a discontinuity between dSphs/dEs and rotating disks. However, at least on the

observational side, this analysis may have to wait for the next generation of telescopes. An initial analysis of one slightly more massive ($M_\star \sim 10^9$ M$_\odot$) simulated dwarf run with the same code at slightly lower resolution, shows that it is also dispersion-supported ($v_{rot}/\sigma \lesssim 0.25$), but more runs at higher mass are needed in the simulations to make a stronger statement about mass trends.

6 DISCUSSION

A clear prediction made by the tidal stirring model of dSph formation is the increase of v_{rot}/σ with increasing distance from a more massive galaxy (Kazantzidis et al. 2011a). Because the most distant galaxies in the Local Group could have had no more than one pericenter passage in a Hubble time (and most are expected to have had none, e.g., Garrison-Kimmel et al. 2014), we would expect that galaxies that lie beyond the virial radius of either giant to have larger v_{rot}/σ values if tidal stirring plays the primary role in shaping dwarf galaxy dynamics.

Figure 3 explores this possibility by showing v_{rot}/σ vs. distance from the closest massive Local Group galaxy (MW or M31). A zoomed-in region is also shown for galaxies within 300 kpc of a giant (with the exception of And II, which was removed for clarity). We do not see any clear trend between v_{rot}/σ and distance to a massive galaxy, as would be expected if multiple close pericenter passages were necessary for removing rotation from dwarf galaxies.

Given the lack of trend between v_{rot}/σ and distance, we are more inclined to suspect that the stars in small galaxies are formed in a medium with at most marginal rotation support. Some further evidence for this comes from Sánchez-Janssen, Méndez-Abreu & Aguerri (2010), who study 11,753 galaxies from the Sloan Digital

---

[6] The simulations also show a higher degree of rotation in their cold gas, in qualitative agreement with observations (Mateo 1998; Grebel 1999).

Sky Survey (SDSS) and Karachentsev et al. (2004). They suggest the existence of a critical stellar mass, $M_\star = 2 \times 10^9$ $M_\odot$, below which all galaxies become systematically thicker. One important question that will need to be investigated with future simulations is whether or not galaxies that start out with $v_{\rm rot}/\sigma \sim 1$ can undergo enough of a transformation to match the near zero values observed for the smallest dwarf satellites. It would be instructive to use dispersion-dominated dwarfs – in particular at slightly higher mass than those presented here – as the initial conditions for tidal-stirring simulations.

We have checked to see if the four observed "rotating" systems are distinct in other properties that might help explain why they have $v_{\rm rot}/\sigma$ values that are > 1. These objects do not appear to be significant outliers in metallicity, inner density, star formation history or star formation rate, but a more thorough search for galaxy properties that do correlate with $v_{\rm rot}/\sigma$ would be useful. In addition to explaining the small number of outlying observed dwarfs, it could further explain why the simulated galaxies fail to demonstrate an elevated $v_{\rm rot}/\sigma$ – perhaps all simulated halos were selected in a way that disfavors the property that best correlates with rotation support.

All stars analyzed in this work are either red giant or horizontal branch stars, so it is unlikely that we are biasing our sample due to stellar ages. A separate analysis of stellar populations with varying ages – in both the observations as well as the simulations – would likely be informative, but is beyond the scope of this paper.

7 SUMMARY AND CONCLUSION

We have performed a systematic Bayesian search for stellar rotation in 40 dwarf galaxies ($10^{3.5}$ $M_\odot$ $< M_\star < 10^8$ $M_\odot$) in the Local Group, using resolved stellar kinematic data from the literature. We find that the vast majority of these galaxies ($\sim 90\%$) have $v_{\rm rot}/\sigma$ values that imply dispersion-supported kinematics. In particular, we find that 7/10 isolated dwarfs in our sample are also dispersion-supported, with $v_{\rm rot}/\sigma < 0.6$, and all have $v_{\rm rot}/\sigma \lesssim 2$ (see Figure 1 and Table 1). This result for the most distant LG dwarfs galaxies contrasts the common assumption that dwarf galaxies form with cold, rotationally-supported stellar disks. We find no strong trend of $v_{\rm rot}/\sigma$ with $M_\star$ within the mass range studied (Figure 2), nor any trend of $v_{\rm rot}/\sigma$ with distance from large host galaxy in the Local Group (Figure 3), as would be expected if tidal stirring scenarios drive a kinematic transformation of stars in dIrr galaxies to dSph galaxies.

Taken together, our results suggest that dwarf galaxies form as puffy stellar systems that are largely dispersion-supported. The conversion of a dIrr galaxy into dSph galaxy may involve little more than the removal of its gas. The mild rotation of the stellar components we see in some dIrr galaxies in our sample could potentially be accommodated in such scenario, as the process of gas striping itself may be enough to shock the potential, transforming a stellar system with $v_{\rm rot}/\sigma \sim 1.5$ into a system with $v_{\rm rot}/\sigma \sim 0.5$. Detailed simulations of this kind will be needed to test this hypothesis.

The formation of initially dispersion-supported systems is more likely to occur within dark matter halos with shallow potential wells (KWB), especially if explosive feedback effects act to dynamically heat stellar populations after the stars form. We have examined $v_{\rm rot}/\sigma$ in four cosmological zoom-in simulations of isolated dwarf galaxies that include such explosive feedback events (Wheeler et al. 2015; Oñorbe et al. 2015; Muratov et al. 2015).

These simulated dwarfs have $M_\star - M_{\rm halo}$ values that lie very close to extrapolated abundance-matching relations (Hopkins et al. 2014; Oñorbe et al. 2015; Wheeler et al. 2015), so the total amount of energy injected to the surrounding medium is likely appropriate. However, the strength and frequency of bursts could modify the fraction of energy that couples to stars and dark matter, and so could be driving the stellar kinematics. The simulated dwarfs have (mock-observed) stellar dispersion support values $v_{\rm rot}/\sigma \simeq 0 - 0.5$ (and ellipticities $\simeq 0.1 - 0.7$) that are completely consistent with our derived properties of observed satellite dwarfs and isolated dwarfs without a significant need for harassment from a massive neighbor. While these simulations are certainly not the final word on the formation of dwarf galaxies, the result suggests that it is at least reasonable to posit that dwarf galaxies are generally born hot and are never strongly rotationally-supported.

The comparison between our model isolated dwarfs and the data did reveal one source of potential tension: none of our simulated dwarfs have stellar rotations that are as high as the highest in our sample (the 3/10 isolated galaxies with $v_{\rm rot}/\sigma \simeq 1.3 - 2$). This is not particularly surprising, given the small number of simulations analyzed here, but if this discrepancy holds in the face of better data and more simulations, it could point to a new test for feedback models. In particular, it is via bursty and violent feedback episodes that the dark matter cores in these halos are reduced in density, thus alleviating potential problems with LCDM like the Too Big to Fail problem (Boylan-Kolchin, Bullock & Kaplinghat 2011). As first pointed out by Teyssier et al. (2013), the same outbursts also inject significant random energy into the stellar populations (see also Chan et al. 2015). A more detailed comparison between simulated and observed $v_{\rm rot}/\sigma$ values may offer an interesting direction in testing models that attempt to solve dark matter problems via explosive feedback episodes (e.g. Governato et al. 2012; Teyssier et al. 2013; Brooks & Zolotov 2014; Oñorbe et al. 2015; Chan et al. 2015). Can these same models preserve the mild stellar rotation that is seen in a minority of isolated dwarfs? Or, is stellar rotation only seen in galaxies with cuspy density distributions, which would be an important prediction of such models? The analysis of observational data provided here will hopefully provide an important benchmark for this question going forward.

REFERENCES

Adén D. et al., 2009, A&A, 506, 1147

Amorisco N. C., Evans N. W., van de Ven G., 2014, Nature, 507, 335

Battinelli P., Demers S., Kunkel W. E., 2006, A&A, 451, 99

Begum A., Chengalur J. N., 2004, A&A, 413, 525

Belokurov V. et al., 2009, MNRAS, 397, 1748

Bender R., Burstein D., Faber S. M., 1993, ApJ, 411, 153

Besla G., Kallivayalil N., Hernquist L., Robertson B., Cox T. J., van der Marel R. P., Alcock C., 2007, ApJ, 668, 949

Binney J., 1978, MNRAS, 183, 501

Blumenthal G. R., Faber S. M., Primack J. R., Rees M. J., 1984, Nature, 311, 517

Boylan-Kolchin M., Bullock J. S., Kaplinghat M., 2011, MNRAS, 415, L40

Boylan-Kolchin M., Bullock J. S., Sohn S. T., Besla G., van der Marel R. P., 2013, ApJ, 768, 140

Brooks A. M., Zolotov A., 2014, ApJ, 786, 87

Cappellari M. et al., 2007, MNRAS, 379, 418

Carlin J. L., Grillmair C. J., Muñoz R. R., Nidever D. L., Majewski S. R., 2009, ApJ, 702, L9

Chan T. K., Kereš D., Oñorbe J., Hopkins P. F., Muratov A. L., Faucher-Giguère C.-A., Quataert E., 2015, MNRAS, 454, 2981

Collins M. L. M. et al., 2010, MNRAS, 407, 2411

Collins M. L. M. et al., 2013, ApJ, 768, 172

Collins M. L. M. et al., 2011, MNRAS, 417, 1170

Dalcanton J. J., Yoachim P., Bernstein R. A., 2004, ApJ, 608, 189

Deason A. J. et al., 2014, MNRAS, 444, 3975

Demers S., Battinelli P., Kunkel W. E., 2006, ApJ, 636, L85

Dinescu D. I., Girard T. M., van Altena W. F., López C. E., 2005, ApJ, 618, L25

D'Onghia E., Besla G., Cox T. J., Hernquist L., 2009, Nature, 460, 605

Dressler A., 1980, ApJ, 236, 351

Faber S. M., Lin D. N. C., 1983, ApJ, 266, L17

Fall S. M., Efstathiou G., 1980, MNRAS, 193, 189

Feast M. W., Thackeray A. D., Wesselink A. J., 1961, MNRAS, 122, 433

Ferguson H. C., Binggeli B., 1994, A&A Rev., 6, 67

Feroz F., Hobson M. P., 2008, MNRAS, 384, 449

Feroz F., Hobson M. P., Bridges M., 2009, MNRAS, 398, 1601

Fillingham S. P., Cooper M. C., Wheeler C., Garrison-Kimmel S., Boylan-Kolchin M., Bullock J. S., 2015, MNRAS, 454, 2039

Fitts A., Boylan-Kolchin M., Bullock J. S., Wheeler C., 2015, in prep.

Fraternali F., Tolstoy E., Irwin M. J., Cole A. A., 2009, A&A, 499, 121

Frinchaboy P. M., Majewski S. R., Muñoz R. R., Law D. R., Łokas E. L., Kunkel W. E., Patterson R. J., Johnston K. V., 2012, ApJ, 756, 74

Garrison-Kimmel S., Boylan-Kolchin M., Bullock J. S., Lee K., 2014, MNRAS, 438, 2578

Geha M., van der Marel R. P., Guhathakurta P., Gilbert K. M., Kalirai J., Kirby E. N., 2010, ApJ, 711, 361

Geha M., Willman B., Simon J. D., Strigari L. E., Kirby E. N., Law D. R., Strader J., 2009, ApJ, 692, 1464

Governato F. et al., 2012, MNRAS, 422, 1231

Grebel E. K., 1999, in IAU Symposium, Vol. 192, The Stellar Content of Local Group Galaxies, Whitelock P., Cannon R., eds., p. 17

Ho N. et al., 2012, ApJ, 758, 124

Hopkins P. F., Kereš D., Oñorbe J., Faucher-Giguère C.-A., Quataert E., Murray N., Bullock J. S., 2014, MNRAS, 445, 581

Hunter D. A., Elmegreen B. G., 2006, ApJS, 162, 49

Ibata R. A., Wyse R. F. G., Gilmore G., Irwin M. J., Suntzeff N. B., 1997, AJ, 113, 634

Icke V., 1985, A&A, 144, 115

Irwin M., Tolstoy E., 2002, MNRAS, 336, 643

Kalirai J. S. et al., 2010, ApJ, 711, 671

Kaplinghat M., Strigari L. E., 2008, ApJ, 682, L93

Karachentsev I. D., Karachentseva V. E., Huchtmeier W. K., Makarov D. I., 2004, AJ, 127, 2031

Kaufmann T., Wheeler C., Bullock J. S., 2007, MNRAS, 382, 1187

Kazantzidis S., Łokas E. L., Callegari S., Mayer L., Moustakas L. A., 2011a, ApJ, 726, 98

Kazantzidis S., Łokas E. L., Mayer L., 2013, ApJ, 764, L29

Kazantzidis S., Łokas E. L., Mayer L., Knebe A., Klimentowski J., 2011b, ApJ, 740, L24

Kepley A. A., Wilcots E. M., Hunter D. A., Nordgren T., 2007, AJ, 133, 2242

Kim D., Jerjen H., 2015, ApJ, 808, L39

Kim D., Jerjen H., Mackey D., Da Costa G. S., Milone A. P., 2015, ApJ, 804, L44

Kirby E. N., Boylan-Kolchin M., Cohen J. G., Geha M., Bullock J. S., Kaplinghat M., 2013, ApJ, 770, 16

Kirby E. N., Bullock J. S., Boylan-Kolchin M., Kaplinghat M., Cohen J. G., 2014, MNRAS, 439, 1015

Kirby E. N., Cohen J. G., Simon J. D., Guhathakurta P., 2015, preprint (arXiv:1510.03856)

Kirby E. N., Simon J. D., Cohen J. G., 2015, ApJ, 810, 56

Kleyna J. T., Wilkinson M. I., Evans N. W., Gilmore G., 2005, ApJ, 630, L141

Klimentowski J., Łokas E. L., Kazantzidis S., Mayer L., Mamon G. A., 2009, MNRAS, 397, 2015

Koch A., Kleyna J. T., Wilkinson M. I., Grebel E. K., Gilmore G. F., Evans N. W., Wyse R. F. G., Harbeck D. R., 2007a, AJ, 134, 566

Koch A., Wilkinson M. I., Kleyna J. T., Gilmore G. F., Grebel E. K., Mackey A. D., Evans N. W., Wyse R. F. G., 2007b, ApJ, 657, 241

Koch A. et al., 2009, ApJ, 690, 453

Koposov S. E., Belokurov V., Torrealba G., Evans N. W., 2015a, ApJ, 805, 130

Koposov S. E. et al., 2015b, ApJ, 811, 62

Koposov S. E. et al., 2011, ApJ, 736, 146

Kormendy J., Fisher D. B., Cornell M. E., Bender R., 2009, ApJS, 182, 216

Laevens B. P. M. et al., 2015a, ApJ, 813, 44

Laevens B. P. M. et al., 2015b, ApJ, 802, L18

Leaman R., Cole A. A., Venn K. A., Tolstoy E., Irwin M. J., Szeifert T., Skillman E. D., McConnachie A. W., 2009, ApJ, 699,

1

Leaman R. et al., 2012, ApJ, 750, 33

Lépine S., Koch A., Rich R. M., Kuijken K., 2011, ApJ, 741, 100

Łokas E. L., Kazantzidis S., Mayer L., 2011, ApJ, 739, 46

Łokas E. L., Semczuk M., Gajda G., D'Onghia E., 2015, ApJ, 810, 100

Martin N. F. et al., 2014, ApJ, 793, L14

Martin N. F., Ibata R. A., Chapman S. C., Irwin M., Lewis G. F., 2007, MNRAS, 380, 281

Martin N. F. et al., 2015a, preprint (arXiv:1510.04433)

Martin N. F. et al., 2015b, ApJ, 804, L5

Martin N. F. et al., 2013, ApJ, 772, 15

Massari D., Bellini A., Ferraro F. R., van der Marel R. P., Anderson J., Dalessandro E., Lanzoni B., 2013, ApJ, 779, 81

Mastropietro C., Moore B., Mayer L., Debattista V. P., Piffaretti R., Stadel J., 2005, in IAU Colloq. 198: Near-fields cosmology with dwarf elliptical galaxies, Jerjen H., Binggeli B., eds., pp. 244–248

Mateo M., Olszewski E. W., Walker M. G., 2008, ApJ, 675, 201

Mateo M. L., 1998, ARA&A, 36, 435

Mayer L., 2010, Advances in Astronomy, 2010, 25

Mayer L., Governato F., Colpi M., Moore B., Quinn T., Wadsley J., Stadel J., Lake G., 2001a, ApJ, 559, 754

Mayer L., Governato F., Colpi M., Moore B., Quinn T., Wadsley J., Stadel J., Lake G., 2001b, ApJ, 547, L123

Mayer L., Mastropietro C., Wadsley J., Stadel J., Moore B., 2006, MNRAS, 369, 1021

McConnachie A. W., 2012, AJ, 144, 4

Moore B., Katz N., Lake G., Dressler A., Oemler A., 1996, Nature, 379, 613

Muñoz R. R., Carlin J. L., Frinchaboy P. M., Nidever D. L., Majewski S. R., Patterson R. J., 2006a, ApJ, 650, L51

Muñoz R. R., Carlin J. L., Frinchaboy P. M., Nidever D. L., Majewski S. R., Patterson R. J., 2006b, ApJ, 650, L51

Muñoz R. R. et al., 2005, ApJ, 631, L137

Muratov A. L., Kereš D., Faucher-Giguère C.-A., Hopkins P. F., Quataert E., Murray N., 2015, MNRAS, 454, 2691

Oñorbe J., Boylan-Kolchin M., Bullock J. S., Hopkins P. F., Kereš D., Faucher-Giguère C.-A., Quataert E., Murray N., 2015, MNRAS, 454, 2092

Oñorbe J., Garrison-Kimmel S., Maller A. H., Bullock J. S., Rocha M., Hahn O., 2014, MNRAS, 437, 1894

Oemler, Jr. A., 1974, ApJ, 194, 1

Pace A., 2015, in prep.

Peñarrubia J., Belokurov V., Evans N. W., Martínez-Delgado D., Gilmore G., Irwin M., Niederste-Ostholt M., Zucker D. B., 2010, MNRAS, 408, L26

Peñarrubia J. et al., 2011, ApJ, 727, L2

Piatek S., Pryor C., Bristow P., Olszewski E. W., Harris H. C., Mateo M., Minniti D., Tinney C. G., 2005, AJ, 130, 95

Piatek S., Pryor C., Bristow P., Olszewski E. W., Harris H. C., Mateo M., Minniti D., Tinney C. G., 2006, AJ, 131, 1445

Piatek S., Pryor C., Bristow P., Olszewski E. W., Harris H. C., Mateo M., Minniti D., Tinney C. G., 2007, AJ, 133, 818

Piatek S., Pryor C., Olszewski E. W., Harris H. C., Mateo M., Minniti D., Tinney C. G., 2003, AJ, 126, 2346

Pryor C., Piatek S., Olszewski E. W., 2010, AJ, 139, 839

Pryor C., Piatek S., Olszewski E. W., 2015, AJ, 149, 42

Rocha M., Peter A. H. G., Bullock J., 2012, MNRAS, 425, 231

Salomon J.-B., Ibata R. A., Martin N. F., Famaey B., 2015, MNRAS, 450, 1409

Sánchez-Janssen R., Méndez-Abreu J., Aguerri J. A. L., 2010, MNRAS, 406, L65

Saviane I., Held E. V., Piotto G., 1996, A&A, 315, 40

Simon J. D., Drlica-Wagner A., Li T. S., Nord B., Geha M., Bechtol K., 2015, ApJ, 808, 95

Simon J. D., Geha M., 2007, ApJ, 670, 313

Simon J. D. et al., 2011, ApJ, 733, 46

Sohn S. T., Besla G., van der Marel R. P., Boylan-Kolchin M., Majewski S. R., Bullock J. S., 2013, ApJ, 768, 139

Starkenburg T. K., Helmi A., Sales L. V., 2015, preprint (arXiv:1508.06281)

Teyssier R., Pontzen A., Dubois Y., Read J. I., 2013, MNRAS, 429, 3068

Tollerud E. J. et al., 2012, ApJ, 752, 45

Tollerud E. J., Geha M. C., Vargas L. C., Bullock J. S., 2013, ApJ, 768, 50

Toloba E. et al., 2014, ApJS, 215, 17

Tolstoy E., Irwin M., 2000, MNRAS, 318, 1241

Tomozeiu M., Mayer L., Quinn T., 2015, preprint (arXiv:1506.02140)

Trotta R., 2008, Contemporary Physics, 49, 71

van den Bergh S., 1999, A&A Rev., 9, 273

van der Marel R. P., Alves D. R., Hardy E., Suntzeff N. B., 2002, AJ, 124, 2639

Walker M. G., Belokurov V., Evans N. W., Irwin M. J., Mateo M., Olszewski E. W., Gilmore G., 2009, ApJ, 694, L144

Walker M. G., Mateo M., Olszewski E. W., 2008, ApJ, 688, L75

Walker M. G., Mateo M., Olszewski E. W., Bailey, III J. I., Koposov S. E., Belokurov V., Evans N. W., 2015, ApJ, 808, 108

Walker M. G., Mateo M., Olszewski E. W., Bernstein R., Wang X., Woodroofe M., 2006, AJ, 131, 2114

Walker M. G., Mateo M., Olszewski E. W., Gnedin O. Y., Wang X., Sen B., Woodroofe M., 2007, ApJ, 667, L53

Walker M. G., Olszewski E. W., Mateo M., 2015, MNRAS, 448, 2717

Wetzel A. R., Deason A. J., Garrison-Kimmel S., 2015, ApJ, 807, 49

Wheeler C., Oñorbe J., Bullock J. S., Boylan-Kolchin M., Elbert O. D., Garrison-Kimmel S., Hopkins P. F., Kereš D., 2015, MNRAS, 453, 1305

White S. D. M., Rees M. J., 1978, MNRAS, 183, 341

Wilkinson M. I., Kleyna J. T., Evans N. W., Gilmore G. F., Irwin M. J., Grebel E. K., 2004, ApJ, 611, L21

Willman B., Geha M., Strader J., Strigari L. E., Simon J. D., Kirby E., Ho N., Warres A., 2011, AJ, 142, 128

Yoachim P., Dalcanton J. J., 2006, AJ, 131, 226

Young L. M., Lo K. Y., 1996, ApJ, 462, 203

Young L. M., van Zee L., Lo K. Y., Dohm-Palmer R. C., Beierle M. E., 2003, ApJ, 592, 111